Observation of high-spin states in the $N=84$ nucleus ^{152}Er and comparison with shell-model calculations

A. Kuhnert,* D. Alber, H. Grawe, H. Kluge, K. H. Maier, W. Reviol,† and X. Sun‡
Hahn-Meitner-Institut Berlin, D-1000 Berlin, Germany

E. M. Beck,§ A. P. Byrne,** and H. Hübel
Institut für Strahlen- und Kernphysik, Universität Bonn, D-5200 Bonn, Germany

J. C. Bacelar,†† M. A. Deleplanque, R. M. Diamond, and F. S. Stephens
University of California, Lawrence Berkeley Laboratory, Berkeley, California 94720
(Received 11 March 1992)

High-spin states in ^{152}Er have been populated through the ^{116}Sn(^{40}Ar,4n)^{152}Er reaction. Prompt and delayed γ-γ-γ-t and γ-e-t coincidences have been measured. Levels and transitions are assigned up to an excitation energy of 15 MeV and spin and parities up to 28^+ at 9.7 MeV. A new isomer [$t_{1/2}=11(1)$ ns] has been observed at 13.4 MeV. The results are discussed in comparison with neighboring nuclei and with shell-model calculations.

PACS number(s): 21.10.Hw, 21.10.Tg, 21.60.Cs, 27.70.+q

I. INTRODUCTION

The nucleus $^{152}Er_{84}$ with six valence nucleons, four protons and two neutrons, above the shell closure at $Z=64$ and $N=82$ shows a spherical shell-model structure up to high spins. Excited states can be generally interpreted as alignments of the high-j particles available just above $N=82$ and $Z=64$ [1]. A detailed measurement of the level scheme gives an opportunity to compare experimental and theoretical excitation energies and to test the shell model for this relatively large number of valence nucleons.

At higher spins the nuclei in this region are expected to undergo a shape transition from spherical shape to small oblate deformation [2,3]. The angular momentum of the nucleus is generated by aligning the spins of the nucleons in shell-model orbitals which results in a polarization of the core to oblate shapes. Irregularities in the yrast line due to shell effects can then lead to high-spin isomeric states. Indeed, ^{152}Er lies in the region with $64\leq Z\leq 71$ and $N\geq 82$, where many long-lived isomers occur [4], and previous measurements [5] have identified two high-spin isomers in ^{152}Er at about 8.5(0.4)-MeV and ≥ 12.2-MeV excitation energy. An accurate determination of the excitation energies and lifetimes of these isomers was one goal of the present experiment. We also searched for superdeformed bands, primarily above the isomers using them as triggers, but superdeformation was not found in this nucleus in this experiment.

Heavy-ion fusion reactions used to produce neutron-deficient rare-earth nuclei lead to a large number of reaction products because of the competing evaporation of charged particles. For the high-spin spectroscopy of these products, the sensitivity and resolution of multidetector arrays of Compton-suppressed Ge detectors is required. Using the high-energy resolution array (HERA), with 21 Ge detectors, at the Lawrence Berkeley Laboratory made it possible to store only threefold and higher-fold γ-ray coincidence events. As discussed below, these data permitted the complex decay to be untangled and to separate contaminants much better than the use of twofold coincidences, and thus allowed the unambiguous placement of transitions with intensities of about 1% of that to the ground state.

The experimental procedures for this investigation of the high-spin states in ^{152}Er are described in Sec. II. The level scheme is discussed in Sec. III. In Sec. IV we compare the experimental results with the excitation structure of the neighboring even-even nuclei and with shell-model calculations using experimental residual interaction energies. A more detailed account of this work is presented in Ref. [6].

II. EXPERIMENTAL TECHNIQUES AND RESULTS

A. Experimental techniques

Three different experiments were performed to determine the level scheme of the neutron-deficient nucleus

*Present address: Lawrence Livermore National Laboratory, Livermore, California 94550.
†Present address: University of Notre Dame, Notre Dame, Indiana 46556.
‡Permanent address: Institute of Modern Physics, Lanzhou, China.
§Permanent address: A. v. Humboldt-Stiftung, D-5300 Bonn, Germany.
**Permanent address: Department of Nuclear Physics, Australian National University, Canberra ACT 2601, Australia.
††Permanent address: University of Netherlands, Groningen, Netherlands.

^{152}Er: γ-ray coincidence measurements using (a) a backed and (b) a thin target, and (c) internal conversion electron measurements. In the first experiment ^{152}Er was produced using the reaction ^{116}Sn(^{40}Ar,4n)^{152}Er* at a projectile energy of 180 MeV at the 88-Inch Cyclotron of the Lawrence Berkeley Laboratory (LBL). The target was a 1.5-mg/cm^2 metallic foil enriched in ^{116}Sn on a 12-mg/cm^2 gold backing. In this reaction the maximum angular momentum transferred to the compound nucleus is $\approx 65\hbar$ and the excitation energy is ≈ 70 MeV. The experimental yield of ^{152}Er amounted to 23% of the fusion cross section in agreement with CASCADE calculations. Additionally, 14 other nuclei from ^{146}Gd to ^{154}Er could be identified in the spectra; their yields varied between 0.3% and 18%; ^{152}Ho and ^{150}Dy were the strongest with intensities of 18% and 15%, respectively. Threefold and higher-fold γ-ray coincidences were measured with HERA, and a total of 3×10^8 threefold coincidences were accumulated. The data acquisition system was limited to three analog-to-digital converters (ADC's) with eight multiplexer channels each which leaves three channels to convert γ-timing information. We divided the 21 Ge detectors into three groups of seven detectors each, and recorded the time of the signal occurring first in a specific detector group relative to the beam pulse. This gives unambiguous time information whenever only *one* detector in a group triggers. Because of the backed target, this experiment was particularly sensitive to γ rays emitted from nuclei at rest, about 1 ps after the reaction.

To look for fast transitions ($t_{1/2} \leq 1$ ps) in the decay of ^{152}Er, a second experiment with a target stack of three 500-μg/cm^2 ^{116}Sn foils was performed. This reduces the width of the velocity distribution of the evaporation residues recoiling into vacuum, and consequently the linewidth of the γ rays emitted in flight. The experiment was carried out at the VICKSI heavy-ion accelerator of the Hahn-Meitner Institute, Berlin using the 12 Compton-suppressed Ge detectors of the OSIRIS array. Twofold and higher-fold coincidences and the time of each detector with respect to the beam burst were recorded. A total of 16×10^7 events were stored on magnetic disk.

For an unambiguous determination of transition multipolarities, especially for the distinction between $M1$ and $E1$ transitions in the range of 5–7-MeV excitation energy, two experiments were performed to measure conversion electrons using a superconducting solenoidal electron spectrometer [7]; γ-e^- coincidences and, for normalization, γ singles were measured. The large number of γ transitions with similar energies in the ^{116}Sn(^{40}Ar,4n)^{152}Er reaction leads to many unresolvable peaks in the electron spectra. Therefore, the reaction ^{114}Sm(^{12}C,4n)^{152}Er was used, resulting in cleaner spectra because of the lower excitation energy and spin for the nucleus. In the first internal conversion electron experiment the Si(Li) detector viewed all electrons directly emitted from the target (1.2-mg/cm^2 ^{144}Sm tilted 20° to the beam). An absorber foil of 3-mg/cm^2 aluminum in front of the detector was used to stop the δ electrons. The γ rays were measured with two Ge detectors positioned at 90° and 135°, respectively. The second experiment utilized the recoil shadow method [8] with the ^{144}Sm(^{13}C,5n)^{152}Er reaction at $E(^{13}\text{C})=95$ MeV. Delayed electrons emitted from recoiling nuclei reach the detector, while the electrons emitted from the target directly were blocked by the baffle. This experiment was sensitive to electrons emitted between 5 and 50 ns after the reaction.

B. Analysis of triple coincidences

The requirement of threefold and higher-fold coincidences discriminates efficiently against low-multiplicity processes such as Coulomb excitation and radioactive decay. It permits the projection of spectra gated by two particular γ transitions and thereby the selection of a single decay path in the desired nucleus even when many transitions are doublets. Figure 1 shows the total projec-

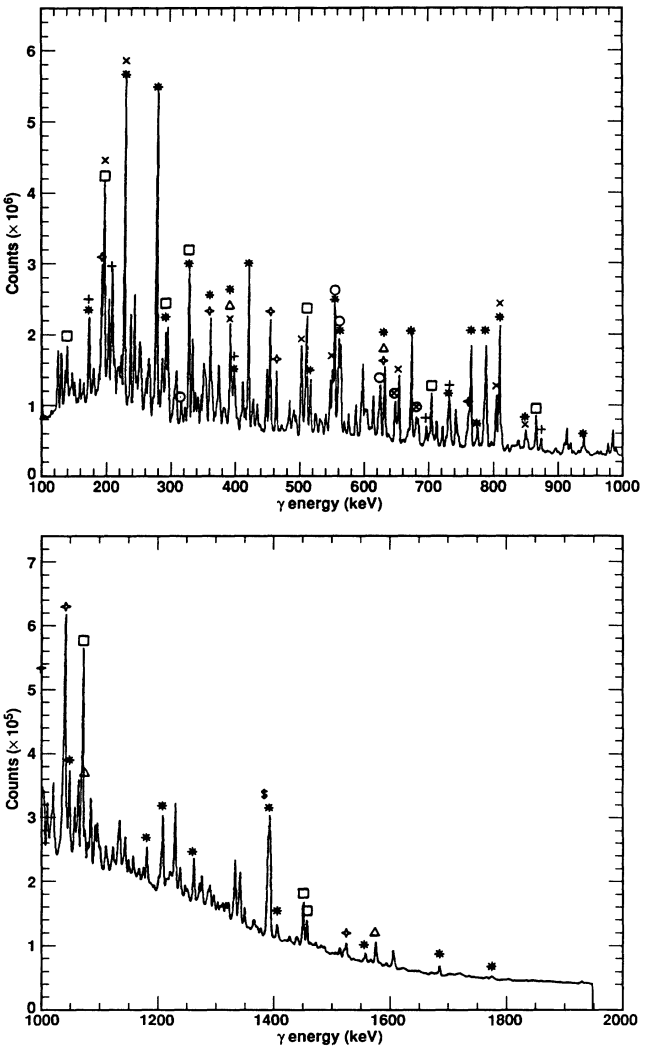

FIG. 1. Total projection of the data obtained with the ^{116}Sn(^{40}Ar,4n)^{152}Er reaction at $E(^{40}\text{Ar})=180$ MeV. The marked lines in the spectrum belong to the following evaporation residues: *, ^{152}Er; +, ^{153}Er; ○, ^{154}Er; $, ^{151}Ho; □, ^{152}Ho; ♦, ^{153}Ho; #, ^{149}Dy; ×, ^{150}Dy; ⊗, ^{152}Dy; △, ^{148,149}Gd.

tion of all coincidence data measured with the reaction ^{116}Sn(^{40}Ar,xn,pxn,αxn). This spectrum contains transitions from all nuclei produced in the fusion reaction. Most of the spectra, which are coincident with one γ transition, show transition from various other evaporation residues while those coincident with two γ transitions are clean. As an example, we show in Fig. 2 spectra single gated on the 395-keV, $18^+ \rightarrow 16^+$ transition, and double gated on the 395- and 729-keV, $19 \rightarrow 18^+$ transitions (see Fig. 9). The latter spectrum contains only transitions in ^{152}Er.

In a first step all fourfold and higher-fold coincidences were broken up into triple coincidences. Then 21 $E\gamma$-$E\gamma$ matrices were sorted with different energy gates on the third γ-ray transition energy involved. No Doppler-shift corrections were necessary for the detectors, which view the target from different angles with respect to the beam axis. This analysis results in sharp lines for γ rays from stopped nuclei only. Figures 3–5 show a representative collection of background-subtracted double-gated coincidence spectra obtained by projecting these matrices with a second energy window.

In the following, some examples which show the advantages of triple coincidences to construct the ^{152}Er level scheme will be discussed using Figs. 3–5. The main difficulty was, as mentioned before, the large number of γ-ray transitions with similar or even equal energies due to the high yield of other evaporation residues. Figure 3 shows the two spectra coincident with the 329.0- and 279.0-keV and with the 329.0- and 720.5-keV transitions, respectively. These transitions are part of the main decay path, therefore, the spectra contain nearly all transitions found in ^{152}Er. The chosen coincidence conditions restrict them exclusively to ^{152}Er and no γ-ray lines from other nuclei appear. The loss in statistics is well compensated by the cleanliness of the spectra obtained. As can be seen in Figs. 4 and 5, triple coincidences allow separation of the different decay paths in ^{152}Er without any con-

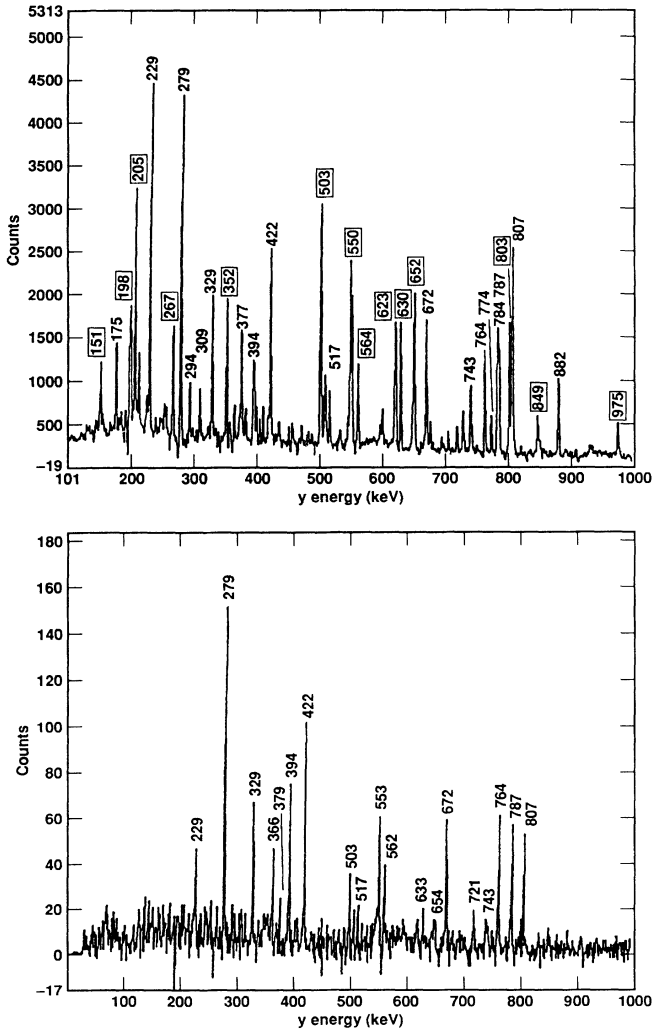

FIG. 2. Top: spectrum obtained by requiring *one* gate at an energy of 395 keV ($18^+ \rightarrow 16^+$). The marked transitions (boxes) do not belong to ^{152}Er. Bottom: Spectrum obtained by requiring *two* gates at energies of 395 ($18^+ \rightarrow 16^+$ transition) and 729.5 keV ($19^- \rightarrow 18^+$ transition). The transition energies marked are within ± 1 keV.

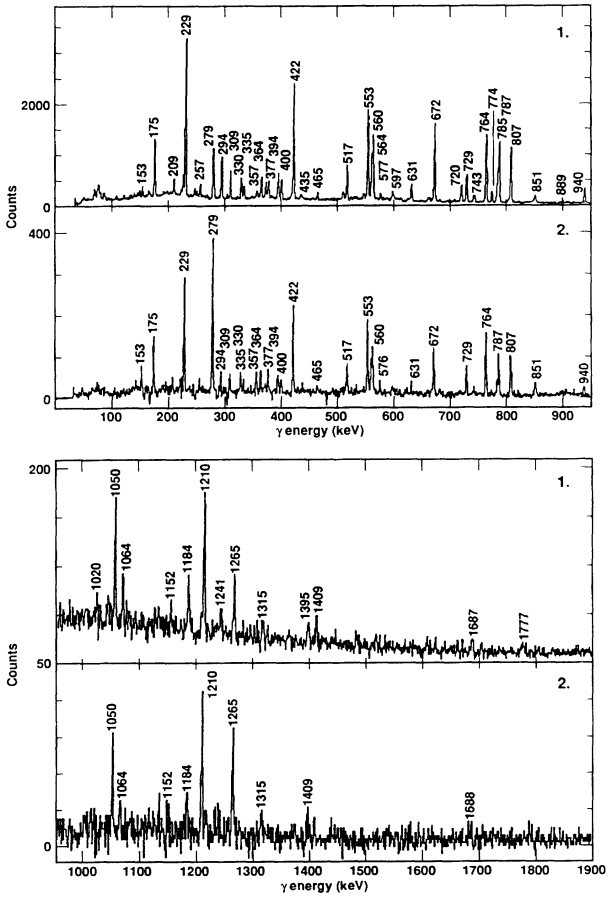

FIG. 3. Spectra obtained by requiring two gates at energies of (1) 329.0 ($24^- \rightarrow 23^-$ transition) and 279.0 keV ($8^+ \rightarrow 6^+$ transition), (2) 329.0 ($24^- \rightarrow 23^-$ transition) and 720.5 keV (at $E_x \approx 12$ MeV), respectively. Shown are the low-energy (top) and high-energy (bottom) parts. The transition energies marked are within ± 1 keV.

tamination. Also, the feeding and depopulation pattern in ^{152}Er results in a greatly increased intensity in the spectra for those transitions which connect the two gate transitions, as shown in Fig. 4, spectra 1 (225.3 keV), 5 (456.0 keV), and 6 (395 keV), and helps to place multiplets in the decay scheme. The unambiguous placement of transitions with intensities less than 1% of that to the ground state, which were very weak in the triple-coincidence spectra, however, were aided by the analysis of single-gated, double-coincidence spectra with their increased statistics. This takes advantage of the fact that 3×10^8 threefold events correspond to 9×10^8 twofold coincidence events.

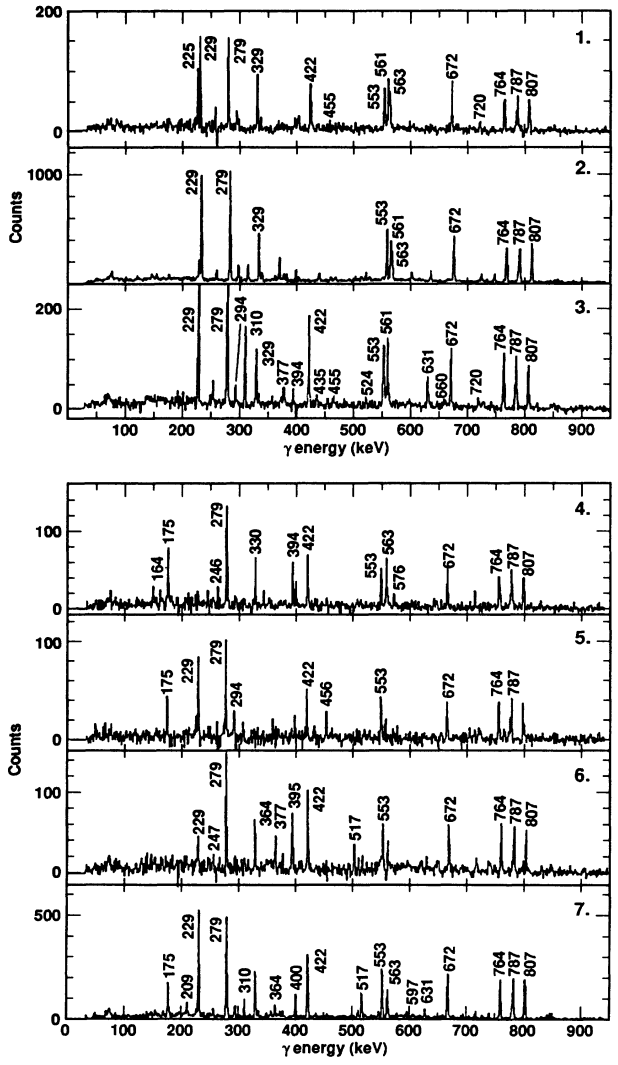

FIG. 4. Spectra obtained by requiring *two* gates at energies of (from top to bottom) (1) 729.5 ($19^-\rightarrow18^+$) and 517.2 keV ($21^-\rightarrow19^-$), (2) 729.5 ($19^-\rightarrow18^+$) and 421.6 keV ($6^+\rightarrow4^+$), (3) 729.5 ($19^-\rightarrow18^+$) and 364.6 keV ($20^-\rightarrow19^-$), (4) 517.2 ($21^-\rightarrow19^-$) and 774.0 keV ($17^-\rightarrow16^+$), (5) 517.2 ($21^-\rightarrow19^-$) and 435.8 keV ($24^-\rightarrow22^-$), (6) 729.5 ($19^-\rightarrow18^+$) and 394.3 keV ($16^+\rightarrow14^+$), and (7) 939.8 ($17^-\rightarrow16^+$) and 174.6 keV ($18^-\rightarrow17^-$). The transition energies marked are within ±1 keV.

From the timing data (Fig. 6), the half-lives of the two high-spin isomers could be determined. The lower one at 9.7-MeV excitation energy shows a half-life of 35(4) ns, comparable to the previously reported 32 ns [9]. The half-life of the high-lying isomer at 13.4 MeV is 11(1) ns. The time spectra of the 1051.0- and 1264.6-keV transitions do not contain a prompt fraction in contrast to the time spectra of the 720.5- and 1210.3-keV (not shown) transitions. Therefore, the 1051.0-keV transition deexcites the 35-ns isomer, and the 1264.6-keV transition deexcites the 11-ns isomer.

The data from the backed-target experiment have also been analyzed by applying a Doppler-shift correction corresponding to the full velocity of the recoiling nuclei. This gives sharp lines for γ rays emitted at times short compared to the slowing-down time of the nuclei (~1 ps). No such lines belonging to ^{152}Er have been found, but in this analysis all the γ rays emitted at rest are smeared out to wide bumps and produce a large background.

C. Transition intensities and γ-γ angular correlation

The intensities of the transitions (Table I) were determined from a spectrum coincident with the 763.6-keV,

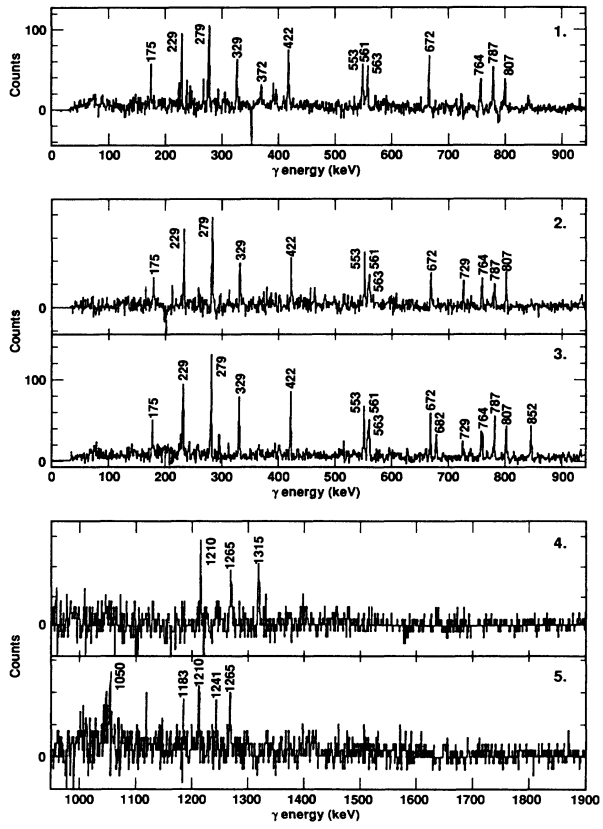

FIG. 5. Spectra obtained by requiring two gates at energies of (from top to bottom) (1) 517.2 ($21^-\rightarrow19^-$) and 255.6 keV (at $E_x\approx8.3$ MeV), (2) and (4) 720.5 (at $E_x\approx12$ MeV) and 357.3 keV (at $E_x\approx10$ MeV), (3) and (5) 720.5 (at $E_x\approx12$ MeV) and 153.3 keV (at $E_x\approx10.5$ MeV). The transition energies marked are within ±1 keV.

$10^+ \rightarrow 8^+$ transition. In the case of multiple peaks or weak transitions, suitable double-gated spectra were used, with a normalization to another transition which could be evaluated in the 763.6-keV gated spectrum. A determination of the γ-ray angular distribution with respect to the beam axis was not possible because the aligned nuclear spins relax rapidly due to their interaction with the fluctuating hyperfine field of the erbium $4f$ electrons. The relaxation time of erbium in lead is given as $\tau_{\text{relax}} = T(\text{K})/3450g^2$ ns [10] (T is the temperature). This means that τ_{relax} is on the order of 100 ps for a g factor of $g = 1$ at room temperature. If we assume that the conditions for erbium in gold are similar, then the existence of two high-lying ns isomers in ^{152}Er destroys the alignment of nuclei passing through the isomers. Indeed, the measured angular distributions are isotropic except for the 329.0- (dipole) and 720.5-keV (quadrupole) transitions for which the analysis indicated strong prompt feeding.

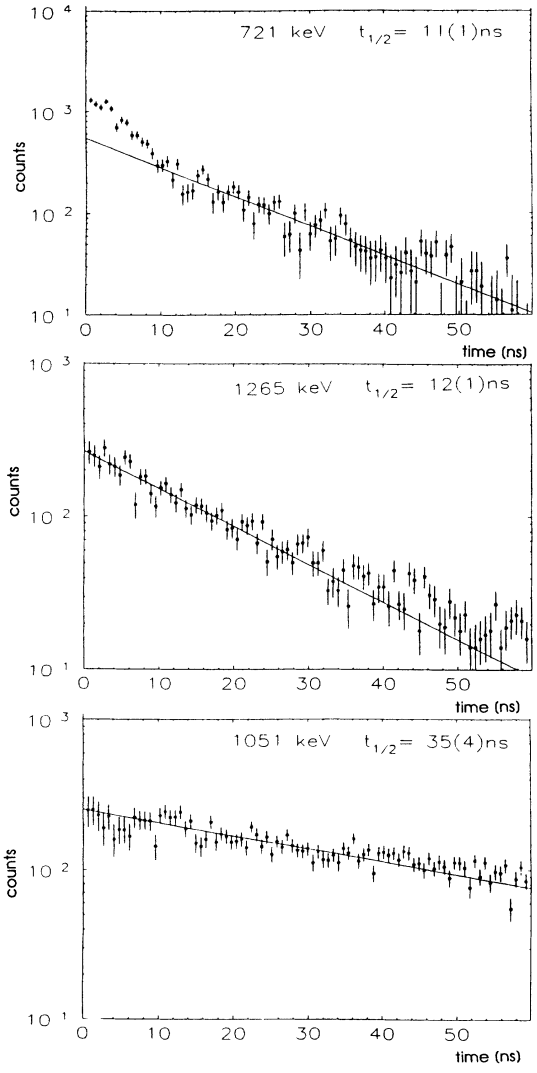

FIG. 6. Time spectra for the 720.5-keV, $E_x \approx 12$ MeV (top), 1264.6-keV, $E_x \approx 13$ MeV (middle), and 1051.0-keV, $28^+ \rightarrow 26^-$ (bottom) transitions in ^{152}Er.

However, it was possible to evaluate the angular correlation between two successive γ-ray transitions emitted from a randomly oriented nucleus. The coincidence rate between pairs of detectors at relative angles close to 90° and close to 30° or 150°, respectively, has been determined. The results for 40 pairs of transitions that populate and depopulate one intermediate state are shown in Fig. 7 and compared with theoretical values. Good agreement is found for the transitions with known multipolarities; the attenuation of the angular correlation of the 560.2- and 229.2-keV pair is caused by the intermediate 16^+ isomer.

Additionally, electron spectra measured in coincidence with several strong γ-ray transitions have been summed to give an electron spectrum relatively free from contamination. From these results and the simultaneously measured γ-ray singles spectrum, the K-conversion coefficients have been determined by normalizing to the clean 421.6-keV, $E2$ transition. The angular correlation data required that the 174.6- and 364.6-keV transitions are of mixed $M1/E2$ multipolarity, and the conversion coefficients agree with this result quantitatively (Table II). As shown in Fig. 8, the absence of K-conversion lines for the 729.5- and 774.0-keV transitions clearly implies $E1$ character; $M1$ transitions would have an about six times larger conversion coefficient and would thus be visible in the spectrum. Therefore, the parity of the levels changes above the 18^+ state. The spin-parity assignments shown in Fig. 9 and Table I were determined from the angular correlation and conversion data with the assumption that stretched quadrupole transitions with energies below 800 keV are of $E2$ character, that stretched dipoles may be either $M1$ or $E1$, and that mixed transitions are of $M1/E2$ type. For the levels up to the 24^- state at 7 MeV, the shown assignments are quite firm, being generally established by different parallel decay paths. At higher energies up to the 28^+ isomer, a complete spin-parity assignment was not possible due to the absence of strong parallel decay cascades.

D. Analysis of the thin-target experiment

The thin-target experiment was performed to investigate fast transitions and possible superdeformation in ^{152}Er. From the analysis of the measured twofold data—gates were set on all known ^{152}Er transitions—we could only deduce levels which show a strong prompt feeding (arrows marked with a "p" in Fig. 9). Additional discrete transitions (which should be sharp if the lifetimes and feeding times are less than 100 ps, the time of flight between two foils) were not found. Setting gates on transitions below the high-spin isomers, such as the 720.5- or the 1210.3- and 329.0-keV transitions, resulted in spectra containing weak or no transitions above them. This is caused by the fact that the recoiling ^{152}Er nuclei left the sensitive volume visible for the detectors before these levels were populated by the decay from the isomeric states. However, these spectra contained most of the ^{152}Er transitions below the gate transitions, which means there must be strong prompt feeding into these states (arrows

TABLE I. Level energies, spins, and parities for the levels observed in ^{152}Er as well as γ energies and γ intensities. *D*, doublet; *M*, multiplet; *N*, not observed, *, taken from [6]. (1) Deviation less than 0.1 keV for strong transitions and up to 0.8 keV for weak high-energy transitions. Comparison with Refs. [1,9] indicates a possible systematic deviation of about -1.0 keV for the γ energies given. (2) From angular correlation and conversion electron measurement. (3) Intensities determined in a spectrum coincident with the 763.7-keV transition. Uncertainty maximal 5% for $I\gamma > 150$, 10% for $I\gamma > 20$, and greater than 20% for $I\gamma < 20$ and $\Delta E < 1.5$ keV. (4) Intensity determined in a spectrum coincident with the 422-keV transition normalized to the strength of the 807-keV transition. (5) Intensity determined in an appropriate double-gated spectrum. (δ) Mixing ratio, in some cases two values agree with the data.

E_x (keV)	$I_1^\pi \rightarrow I_2^\pi$	E_γ (keV)[1]	Multipolarity[2]	$I\gamma$[3]
807.3	$2^+ \rightarrow 0^+$	807.3	$E2^*$	1 000
1 479.0	$4^+ \rightarrow 2^+$	671.7	$E2^*$	973
1900.6	$6^+ \rightarrow 4^+$	421.6	$E2^*$	936
2179.6	$8^+ \rightarrow 6^+$	279.0^D	$E2^*$	1007
2943.2	$10^+ \rightarrow 8^+$	763.4	$E2^*$	965[4]
3729.7	$12^+ \rightarrow 10^+$	786.5	$E2^*$	971
4283.0	$14^+ \rightarrow 12^+$	553.3	$E2$	937
4512.2	$16^+ \rightarrow 14^+$	229.2	$E2$	648
4529.1	$15^+ \rightarrow 14^+$	246.1	$M1$	38
4677.2	$16^+ \rightarrow 15^+$	148.2	$M1$	38
	$16^+ \rightarrow 16^+$	164.9	$M1E2$ $\delta=2/-3.5$	23
	$16^+ \rightarrow 14^+$	394.4^D	$E2$	105
5072.4	$18^+ \rightarrow 16^+$	395.0^D	$E2$	60
	$18^+ \rightarrow 16^+$	560.2	$E2$	490
5405.8	$?\rightarrow 18^+$	333.4		12
5452.0	$17^- \rightarrow 16^+$	774.0	$E1$	115
	$17^- \rightarrow 16^+$	939.8	$E1$	235
5626.6	$18^- \rightarrow 17^-$	174.6	$M1E2$ $\delta=0.2$	201
5802.0	$19^- \rightarrow 18^-$	175.4	$M1$	61
	$19^- \rightarrow 18^-$	729.5	$E1$	392
5957.0	$?\rightarrow 18^-$	330.4		55
6027.1	$19^- \rightarrow 19^-$	225.3	$M1E2$ $\delta=-1.0/1.5$	79
	$19^- \rightarrow 18^-$	400.5	$M1$	143
	$19^- \rightarrow 17^-$	576.1	$E2$	72
6166.6	$20^- \rightarrow 19^-$	139.5	$M1$	6
	$20^- \rightarrow ?$	208.7		48
	$20^- \rightarrow 19^-$	364.6	$M1E2$ $\delta=4.0$	162
6397.5	$?\rightarrow 19^-$	595.5		19
6466.8	$20^- \rightarrow 18^+$	1 394.4^D	$M2$	50
6476.4	$21^- \rightarrow 20^-$	309.8	$M1$	160
6544.3	$21^- \rightarrow 21^-$	67.7[5]	$M1$	17[5]
	$21^- \rightarrow ?$	146.6		5
	$21^- \rightarrow 20^-$	377.8	$M1$	84
	$21^- \rightarrow 19^-$	517.2	$E2$	285
	$21^- \rightarrow 19^-$	243.3	$E2$	107
6722.8	$?\rightarrow 20^-$	256.0^D		100
6827.0	$22\rightarrow 20^-$	660.4	$E2$	38
6745.4	$22\rightarrow ?$	278.0^M		
7001.4	$22^- \rightarrow 21^-$	456.0	$M1$	52
	$22^- \rightarrow 21^-$	523.9	$M1E2$ $\delta=1.0$	36
	$22^- \rightarrow 20^-$	533.4	$E2$	30
	$22^- \rightarrow ?$	1595.6		10
7107.2	$23^- \rightarrow 22^-$	280.4	$M1$	57
	$23^- \rightarrow 21^-$	562.9	$E2$	475
	$23^- \rightarrow 21^-$	630.9	$E2$	140
7436.2	$24^- \rightarrow 23^-$	329.0	$E2$	472
	$24^- \rightarrow 22^-$	435.8	$E2$	97
8099.7	$?\rightarrow 24^-$	663.5		32
8219.9	$26^- \rightarrow ?$	119.5		15
	$26^- \rightarrow 24^-$	783.7	$E2$	255

Table I. (*Continued*).

E_x (keV)	$I_1^\pi \rightarrow I_2^\pi$	E_γ (keV)[1]	Multipolarity[2]	$I\gamma$[3]
8336.9	?→24^-	900.7		27
8475.5	?→26^-	255.6^D		88
8501.8	25→24	1065.6	Dipole	27
	25→23^-	1394.0^D	Quadrupole	
8513.6	27→?	176.5		7
	27→26^-	293.7		181
8646.5	26^-→24^-	1210.3	$E2$	123
8677.9	?→24^-	1241.7		11
8842.2	?→?	372.7		69
	?→27	334.6		77
9665.3	?→27	1151.7		25
9697.5	28^+→?	847.4		38
	28^+→?	1020.1		11
	28^+→26^-	1051.0	$M2E3$ $\delta=-1.5$	96
	28^+→27	1183.2		57
9710.5	?→28^+	$\sim 14^N$		?
10067.8	?→?	357.3^D		48
10290.6	?→?	625.9		16
	?→?	1777.0		10
10379.3	?→?	681.8		37
10532.6	?→?	153.3	($\Delta I=1$)	42
	?→?	464.7		37
	?→?	821.7		25
11106.2	?→?	814.0		21
	?→?	1408.7		25
11383.7	?→?	277.5^M		
	?→?	851.1	($\Delta I=2$)	93
	?→?	1315.2		23
	?→?	1686.2		22
12104.2	?→?	720.5	($\Delta I=2$)	170
13011.6	?→?	907.4		17
13368.8	?→?	357.0^D		
	?→?	1264.6	($\Delta I=3$)	71
14925.9	?→?	1556.8		7

marked with a "p" in Fig. 9). To look for a superdeformed rotational band in ^{152}Er, the measured coincidences were sorted into an E_γ-E_γ-correlation matrix. Neither in the background-subtracted correlation matrix nor in a diagonal cut of the raw data matrix between 900 and 1300 keV (Fig. 10) could any indication for a superdeformed rotational band be found.

III. LEVEL SCHEME OF ^{152}Er

From previous measurements ^{152}Er levels up to 7-MeV excitation energy [1] and up to the 35-ns isomer [9], respectively, were known. The analysis of the triple coincidences, measured with the HERA setup, gave a large number of new transitions resulting in levels up to 15 MeV of excitation energy, as well as to a revision of the transition sequences above $14\hbar$. The exact energy of the 28^+, 35-ns isomer could be determined with the more complete information about its decay, and a new high-spin isomer was found at $E_x=13.4$ MeV with $t_{1/2}=11(1)$ ns, perhaps the highest excitation energy of an isomeric state found so far. Figure 9 shows the level scheme of ^{152}Er, and a compilation of the observed level properties is given in Table I including spins, parities, intensities, and branching ratios. A few critical points on the assignments will be discussed below.

Below 10-MeV excitation energy we found several parallel decay paths besides the main decay already seen in other work [1,9]. Therefore, the order of the transitions and the shown spins and parities are well established in the region 4–10 MeV. But all γ-ray transitions up to spin $14\hbar$ have the same intensities, and no parallel decay path has been observed, so that an unambiguous determination of their order is not possible from the present work. However, the isomeric nature of the 8^+ level and the β decay of ^{152}Tm to it distinguish clearly between transitions above and below that level. The ordering of individual transitions below the 14^+ state is then based on a comparison with neighboring nuclei, particularly ^{150}Dy (Fig. 11) and is the same as in previous studies [1,9].

It is not possible to evaluate the γ-γ angular correlation across the 35-ns isomer because of the earlier-mentioned relaxation time of about 100 ps. But above

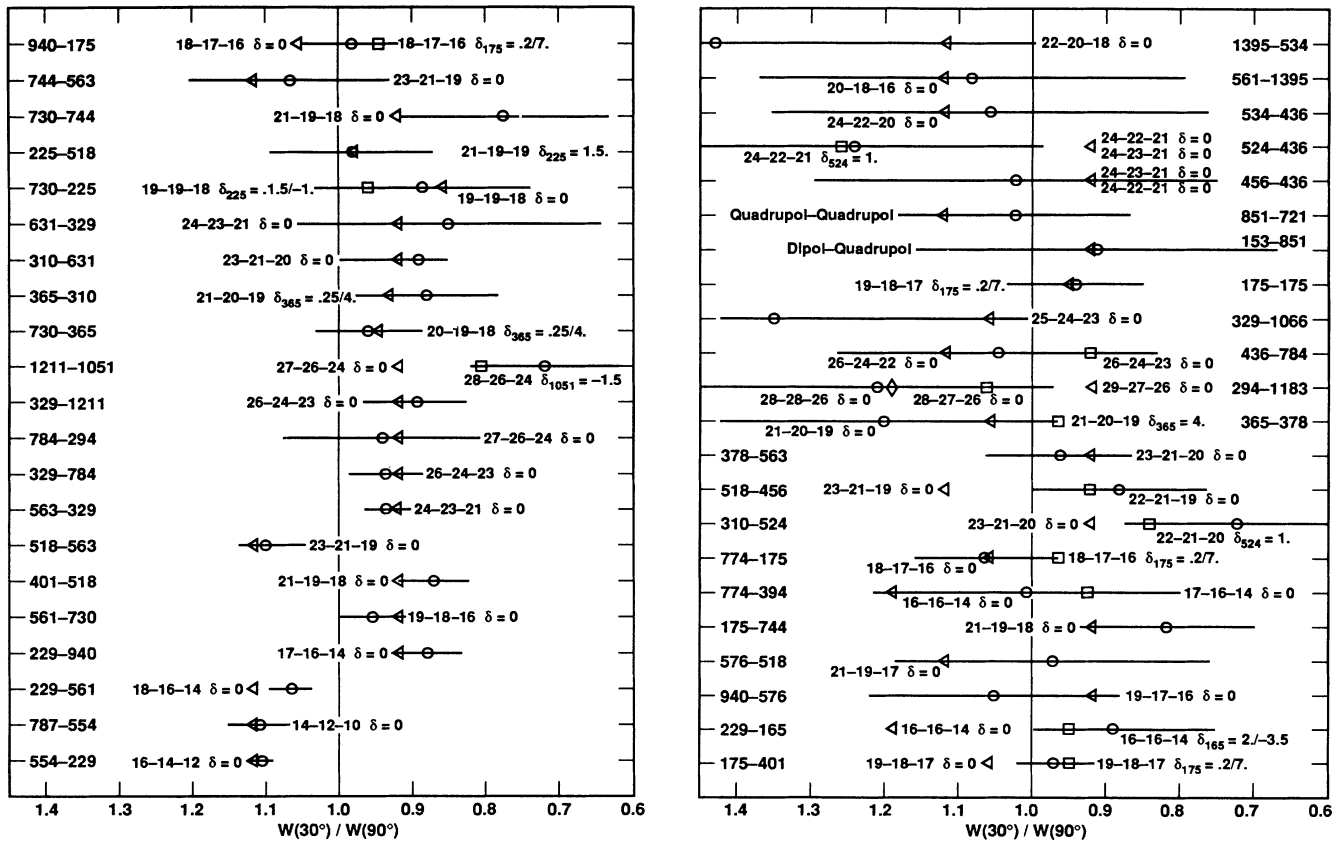

FIG. 7. (a) and (b) Experimental (○) and theoretical (△,□,◆) ratios $W(30°/150°)/W(90°)$ of the coincidence rate for pairs of Ge detectors at relative angles close to 30° or 150°, and close to 90° (angular correlation). Listed are the ratios for 40 pairs of two consecutive γ transitions in ^{152}Er with their energies given in keV. The spin sequences $I_i-(\gamma_{\text{top}})-I_m-(\gamma_{\text{bottom}})-I_f$ for pairs E_γ(bottom)$-E_\gamma$(top) are given for the theoretical ratios (△,□,◆), which in some cases include mixing for one of the involved transitions, i.e., $\delta(E2/M1)$ or $\delta(E3/M2)$. The spin assignments in the level scheme (Fig. 9) reflect the best agreement between the experimental and theoretical ratios and is consistent in case of parallel decay paths.

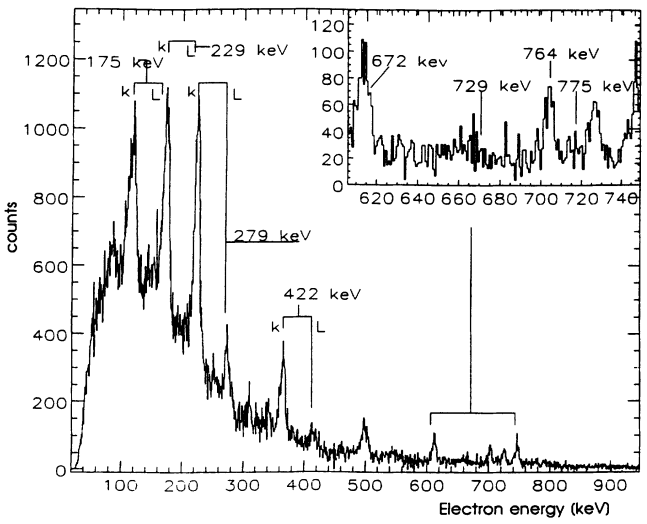

FIG. 8. Electron spectrum in coincidence with several strong γ transitions in ^{152}Er following the reaction ^{144}Sm(^{12}C, $4n$). Inset: The energy range between 600 and 750 keV with γ energies marked for the position of K-conversion lines.

this isomer we could determine the angular distribution of the 720.5-keV transition because of the strong prompt feeding into this level. With the result of $\Delta I=2$ for this transition, it became possible to analyze the angular correlation between the 720.5-keV transition and the 153.3-, 851.1-, and 1264.6-keV transitions. The results suggest $\Delta I=1$ for the 153.3-keV, $\Delta I=2$ for the 851.1-keV, and $\Delta I=3$ for the 1264.6-keV transition (Fig. 7).

IV. DISCUSSION

A. Comparison with neighboring nuclei

The nuclei close to $Z=64$ and $N=82$ reveal, up to a spin of about $40\hbar$, an excitation structure that strongly depends on the nucleon number. With increasing neutron number, the structure changes its pattern from few-particle excitations through vibrational excitations, to collective rotation for $N\geq 90$. In ^{152}Er, with 84 neutrons, the yrast structure is irregular. This can be understood, up to the 28^+ isomer, by the coupling of the six valence nucleons in the available high-spin orbitals: $\pi h_{11/2}$, $\nu f_{7/2}$, $\nu h_{9/2}$, and $\nu i_{13/2}$, and the most

probable configuration for that isomer is $((\pi(h_{11/2})^4)_{16^+}[\nu(i_{13/2})^2]_{12^+}]_{28^+}$.

Comparing the level schemes of ^{152}Er and ^{148}Gd [11], which has only two neutrons outside the $N=82$ shell closure, suggests the configuration $\nu(f_{7/2})^2$ for the levels 0^+ to 6^+ and $\nu f_{7/2}h_{9/2}$ for the 8^+ state (Fig. 11). The 10^+ level then could be a proton $(h_{11/2})^2$ state, as it is seen in ^{148}Dy [12] and ^{150}Er [13]. Higher excitations up to 18^+ can be interpreted as a coupling of the two-proton 10^+ state and the two-neutron 2^+ to 8^+ levels. This is evident from a comparison with ^{150}Dy [14], and from the similarity of the ^{152}Er 10^+ to 18^+ levels and the 0^+ to 8^+ states. The strong similarity in the excitation structure between ^{152}Er and ^{150}Dy (two protons less) shows that the levels up to $I=21$ are built with a proton seniority $v=2$ in ^{152}Er. The only difference is the parity of the $I=17$ state for which we obtain negative parity whereas positive parity is assigned in Ref. [14]. The change in parity above the 18^+ level can be explained with the excitation of one neutron into the $i_{13/2}$ orbital.

B. Shell-model calculations

To determine the configurations for the levels above the $I=21$ state and to show the applicability of the shell model for six valence nucleons, we calculated the energies for the levels using experimental single-particle and residual interaction energies. The results of these calculations agreed with the configurations assigned to the low-lying levels by comparing ^{152}Er with its neighboring nuclei.

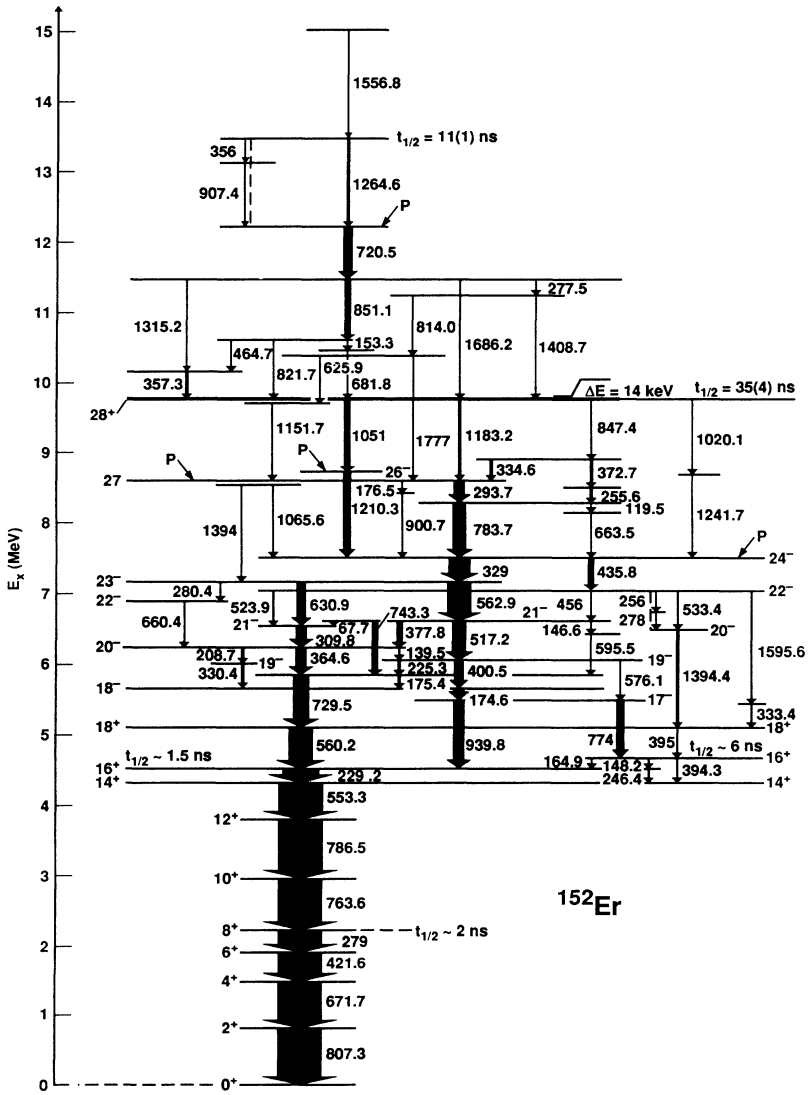

FIG. 9. The ^{152}Er level scheme. The widths of the transition arrows are proportional to the γ-ray intensities observed in the ^{116}Sn(^{40}Ar,4n) reaction. Dashed lines mark ambiguous transition sequences and arrows marked with a p denote strong prompt feeding into this level. The uncertainties for the γ energies given are less than 0.1 keV for the strong transitions, and up to 0.8 keV for weak high-energy transitions. Comparison with Refs. [1,9] indicates a possible systematic deviation of about -1.0 keV for the γ energies given.

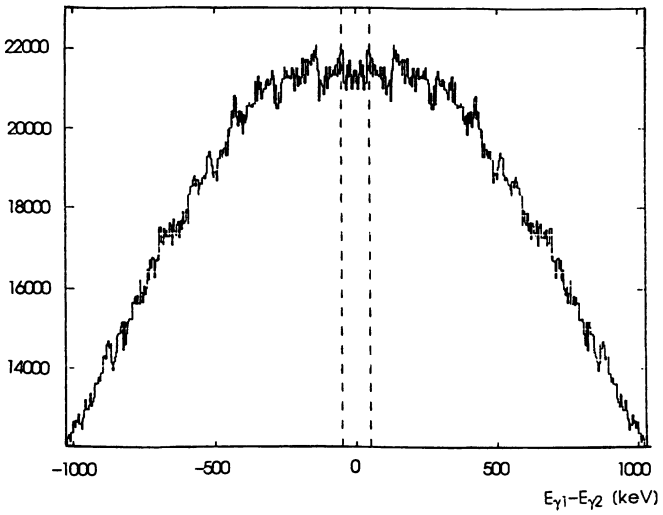

FIG. 10. Projection of the raw data correlation matrix on an axis perpendicular to the matrix diagonal in the energy range from 900 to 1300 keV. The width of the valley, only seen in the energy range from 1.0 to 1.1 MeV, is 98.2 keV.

Table III contains the single-particle energies and Table IV the residual-interaction energies which were used to calculate the level energies for the possible coupling of the six valence nucleons.

TABLE II. Experimental and theoretical K conversion coefficients for certain transitions in ^{152}Er (see text), and α_K/α_L ratio for the 421.6-keV reference transition. Bold multipolarities are in agreement with the angular correlation results.

γ energy (keV)	α_K (expt.)	α_K (theo.)	Multipolarity
560.2	0.012(2)	0.0107	**E2**
729.5	0.007(3)	0.0024	**E1**
		0.0128	**M1**
939.8	0.0012(4)	0.0015	**E1**
		0.0069	**M1**
174.6	0.536(4)	0.5350	**M1E2** $\delta=0.2$
		0.0642	**E1**
		0.5460	**M1**
774.0	0.0038(11)	0.0021	**E1**
		0.0107	**M1**
364.6	0.034(8)	0.0342	**M1E2** $\delta=4.0$
		0.0107	**E1**
		0.0749	**M1**
562.9	0.009(3)	0.0107	**E2**
148.2	0.63(19)	0.8540	**M1**
		0.1030	**E1**
164.9	0.98(78)	0.3660	**M1E2** $\delta=2.0$
		0.0770	**E1**
		0.6310	**M1**
229.2	0.138(21)	0.1160	**E2**
395.0	0.052(17)	0.0086	**E1**
		0.0257	**E2**
		0.0599	**M1**
421.6	$\alpha_K/\alpha_L=5.2\pm1.4$	$\alpha_K/\alpha_L=4.5$	**E2**

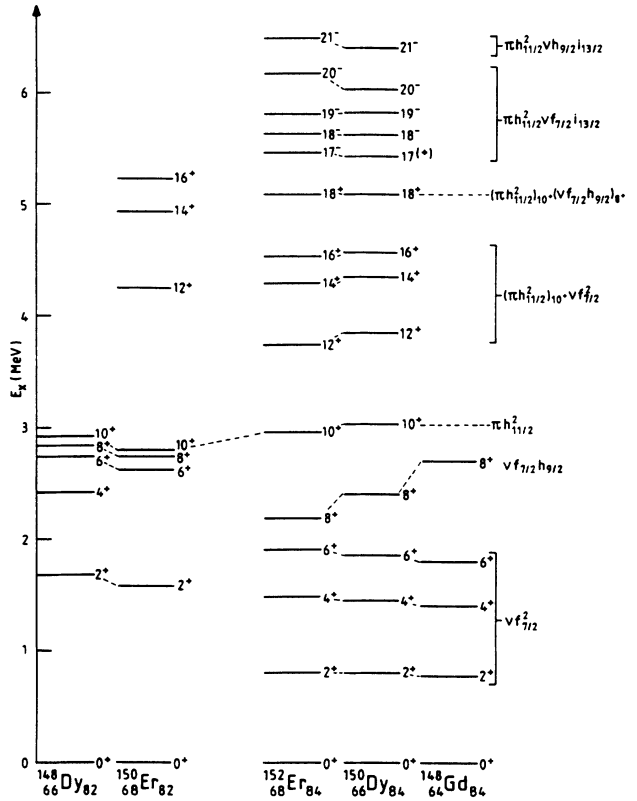

FIG. 11. Comparison between the level schemes for the even-even nuclei close to ^{152}Er and ^{152}Er. Stated are the spin and the parity for each level and its configuration (for references see text). The configurations stated contain the nucleons which are not coupled to $I=0$.

The single-particle energies for the $h_{9/2}$ and $i_{13/2}$ neutrons follow from the $\nu f_{7/2}$ single-particle energy $E_{sp}(\nu f_{7/2})=\Delta^{147}\mathrm{Gd}(\frac{7}{2}^-)$ [20]$-[\Delta^{146}\mathrm{Gd}(0^+)$ [15]$+\Delta n]$, with Δ being the mass, plus the excitation energy of the $I^\pi=\frac{9}{2}^-$ and $I^\pi=\frac{13}{2}^+$ states in ^{147}Gd, respectively. A problem is a significant contribution of $(f_{7/2}\otimes 3^-)_{13/2^+}$ to the $i_{13/2}$ level on the order of 50% [3].[1] Therefore, the stated value does not reflect the true single-particle energy for the $i_{13/2}$ neutron. It is rather an effective energy $E_{sp}(\nu i_{13/2})^*$ used to calculate the levels with negative parity in ^{152}Er assuming a similar admixture of

TABLE III. Single-particle energies for the nucleons outside the ^{146}Gd core.

Particle	Shell-model state	Single-particle energy (keV)	Ref.
Proton	$h_{11/2}$	$-1909(28)$	[15,16]
Neutron	$f_{7/2}$	$-7341(4)$	[15,16]
	$h_{9/2}$	$-5943(4)$	[15,16,3]
	$i_{13/2}$	$-6342(4)$	[15,16,3]

[1]See text for detailed discussion.

$(\nu f_{7/2}\otimes 3^-)_{13/2^+}$ to these levels. Using this effective single-particle energy will result in deviations between the experimental and calculated level energies, since the assumption of almost equal octupole admixture is not strictly fulfilled. In particular, this admixture is blocked for certain levels by the Pauli principle. The 10^- state in ^{148}Gd [11], which is 972 keV above the mixed 9^- state, is an example for such a Pauli blocking of the 3^- admixture. In this case the octupole admixture is blocked because the maximal spin for $[\nu(f_{7/2})^2\otimes 3^-]$ is $I=9$. From the energy of this 10^- state we get a $\nu i_{13/2}$ single-particle energy which is about 1.1 MeV larger than stated in Table II, namely, $E_{sp}(i_{13/2})\approx -5242$ keV. The mixing between $i_{13/2}$ and $(f_{7/2}\otimes 3^-)_{13/2}$ has been explicitly included in calculations for nuclei around ^{208}Pb [21]. It has also been discussed for the nuclei with one to three particles outside the ^{146}Gd core: ^{147}Gd [22], ^{148}Gd [23], and ^{149}Tb [24]. However, for the present case with six particles outside the ^{146}Gd core it is not feasible to include the octupole state explicitly; therefore, all calculations done for configurations which include an $i_{13/2}$ neutron are less reliable. An octupole admixture to the $\frac{7}{2}^-$ ground state in ^{147}Gd is negligibly small due to the large energy difference between the pure $f_{7/2}$ level and the mixed $(i_{13/2}\otimes 3^-)_{7/2^-}$ level. Furthermore, the admixture

TABLE IV. Two-particle residual-interaction energies for the valence nucleons in ^{152}Er.

Shell-model configuration	Spin I^π	Residual interaction (keV)	Ref.
$\pi(h_{11/2})^2$	0^+	−2563(116)	^{148}Dy [12]
	2^+	−885(116)	
	4^+	−135(116)	
	6^+	+169(116)	
	8^+	+271(116)	
	10^+	+357(116)	
$\nu(f_{7/2})^2$	0^+	−1642(12)	^{148}Gd [11]
	2^+	−858(12)	
	4^+	−226(12)	
	6^+	+169(12)	
$\nu f_{7/2}h_{9/2}$	1^+	−298	^{148}Gd [11]
	2^+	−178	
	3^+	−250	
	4^+	−170	
	5^+	−171(12)	
	6^+	−257(12)	
	7^+	−105(12)	
	8^+	−347(12)	
$\nu f_{7/2}i_{13/2}$	3^-	−1367(12)	^{148}Gd [11]
	4^-	−727(12)	
	5^-	−558(12)	
	6^-	−73(12)	
	7^-	−77(12)	
	8^-	+389(12)	
	9^-	+54(12)	
	10^-	+1026(12)	
$\nu h_{9/2}i_{13/2}$	2^-	−280	Kuo-Herling
	3^-	−70	^{206}Pb [17], 2^- to 10^-
	4^-	+70	^{148}Gd [11], 11^-
	5^-	+90	
	6^-	+130	
	7^-	+110	
	8^-	+150	
	9^-	+60	
	10^-	+160	
	11^-	−338	
$\nu(i_{13/2})^2$	0^+	−1409	Kuo-Herling
	2^+	−1003	^{206}Pb [17]
	4^+	−285	
	6^+	−27	
	8^+	+27	
	10^+	+108	
	12^+	+190	
$\pi h_{11/2}\nu f_{7/2}$	2^+	−407(62)	^{148}Tb [18], ^{146}Eu [19]
	3^+	−302(62)	
	4^+	−240(62)	
	5^+	−258(62)	
	6^+	−245(62)	
	7^+	−256(62)	
	8^+	−178(62)	
	9^+	−494(62)	
$\pi h_{11/2}\nu h_{9/2}$	1^+	−1170	Kuo-Herling
	2^+	−824	^{206}Tl [17]
	3^+	−404	
	4^+	−544	
	5^+	−174	
	6^+	−284	
	7^+	−105	
	8^+	−324	
	9^+	−94	
	10^+	−614	
$\pi h_{11/2}\nu i_{13/2}$	1^-	−731	Kuo-Herling
	2^-	−447	^{206}Tl [17]
	3^-	−366	
	4^-	−54	
	5^-	−190	
	6^-	−379	
	7^-	−136	
	8^-	−68	
	9^-	−81	
	10^-	−54	
	11^-	−108	
	12^-	−840	

$(h_{9/2}\otimes 3^-)_{13/2^+}$ or $(i_{13/2}\otimes 3^-)_{9/2^-}$, respectively, is expected to be weak since a spin flip is involved. Therefore, we consider the neutron single-particle energies, determined from the $I^\pi=\frac{9}{2}^-$ and $I^\pi=\frac{7}{2}^-$ levels in ^{147}Gd as reliable, as well as the $\pi h_{11/2}$ single-particle energy derived from the ^{147}Th mass.

To determine the $\nu f_{7/2}$ residual-interaction energy, the known states $I=0-6$ in ^{148}Gd have been used. The values for the $\nu f_{7/2}h_{9/2}$ interaction energy for $I=5-8$ have been taken directly from the corresponding levels in ^{148}Gd [11]. Since the levels with $I=1-4$ are not known in ^{148}Gd, we compare the trends of the interaction energies for $\nu f_{7/2}h_{9/2}$, $I=5-8$ and for the $f_{7/2}h_{9/2}$ neutron-hole configuration in ^{206}Pb, calculated by Kuo and Herling [17], to obtain the residual interaction energies for the coupling to $I=1-4$. Also, the levels with $I=3-10$, belonging to the configuration $\nu f_{7/2}i_{13/2}$, are known in ^{148}Gd [11]. Except for the $I=10$ state, they contain an $(f_{7/2}\otimes 3^-)_{13/2^+}$ admixture to the pure $i_{13/2}$ neutron. We used the excitation energies of these levels to obtain an effective residual-interaction energy for the coupling to $I=3-9$, taking the possible admixture into consideration empirically. The value for $(\nu f_{7/2}i_{13/2})_{10^-}$ in Table IV is strongly repulsive and will correct for the effective $i^*_{13/2}$ single-particle energy when used to calculate levels which do not contain an octupole admixture, i.e., $([\pi(h_{11/2})^2]_{10^+}\otimes(\nu f_{7/2}i_{13/2})_{10^-})$.

The octupole excitation in ^{146}Gd is not a pure collective excitation of the nucleus. It contains on the order of 40–60 % of the particle-hole component $\pi h_{11/2}(d_{5/2})^{-1}$. The interaction between the valence nucleons and this particle-hole component should alter the effect of the octupole admixture to the level energies in nuclei with more valence nucleons. The known energies of the 3^- excitations in the nuclei near ^{146}Gd show that two more protons increase the octupole excitation energy by about 100 keV while two more neutrons lead to a decrease of about 300 keV. Large changes occur again at extreme spins due to the Pauli principle. For the $\frac{17}{2}^+$ level in ^{147}Tb, with the configuration $(\pi h_{11/2}\otimes 3^-)_{17/2^+}$ [25], the $\pi h_{11/2}(d_{5/2})^{-1}$ component of the octupole is blocked because the configuration $\pi h^2_{11/2}d^{-1}_{5/2}$ cannot couple to $I=\frac{17}{2}$ ($I_{\max}=15/2$; $[j(\frac{11}{2})$ and $j(\frac{5}{2})$ must be antiparallel to couple to $I=3]$). Effects like this also occur in ^{152}Er, only somewhat more hidden: for example, when an octupole excitation $\nu f_{7/2}\otimes 3^-$ couples to the $h_{11/2}$ protons.

The $\nu h_{9/2}i_{13/2}$ interaction can be determined from experimental data for the coupling to $I=11$ only ($I=11^-$ level in ^{148}Gd [11]). For $I=2-10$, we took the theoretical data from Kuo and Herling for the configuration $\nu(h_{9/2})^{-1}(i_{13/2})^{-1}$ in ^{206}Pb [17]. For the $\nu i^2_{13/2}$ interaction energy we took the theoretical values from the neutron holes in ^{206}Pb, normalized with the mass ratio 206/152, as no states are known in the neighboring nuclei. The proton-neutron interaction energies $\pi h_{11/2}\nu f_{7/2}$ have been determined from the energy of the 7^+, 8^+, and 9^+ levels in ^{148}Tb [18]. With the energy differences for the $I=2,3,5,6$ levels in ^{146}Eu [19] relative to the known 9^+ state in ^{146}Eu, the interactions for the coupling to these spins have been determined. For $I=4$ we adjusted the interaction to the trend of the interaction energies obtained for the other spins. Adapting the calculated interaction energies for the $\pi(h_{11/2})^{-1}\nu(h_{9/2})^{-1}$ configuration in ^{206}Tl [17] to the excitation energies of the 8^+ and 18^+ states in ^{150}Dy and to the $\frac{9}{2}^-$ state in ^{149}Dy, resulted in the values for the $\pi h_{11/2}\nu h_{9/2}$ interaction. And for $E_{\rm RI}(\pi h_{11/2}\nu i_{13/2})$ we used the theoretical Kuo-Herling values for the $\pi(h_{11/2})^{-1}\nu(i_{13/2})^{-1}$ configuration in ^{206}Tl, normalized with 206/152.

Figure 12 shows experimental and calculated level energies for ^{149}Dy, ^{150}Dy, and ^{150}Er. The calculations have been done to test the single-particle and interaction energies used. The uncertainties in the calculated level energies, relative to the ground state of ^{146}Gd, is the sum of the uncertainties listed in Tables III and IV. Levels which all belong to one configuration have smaller relative uncertainties because the residual interactions for the different coupling of the nucleons have been taken from the known level energies. These are accurate within ± 1.5 keV. The levels involving $i_{13/2}$ neutrons have a large uncertainty due to the unknown strength of the octupole admixture $(f_{7/2}\otimes 3^-)$ in the different nuclei. However, the good agreement between the experimental and calculated level energies in ^{149,150}Dy shows the quali-

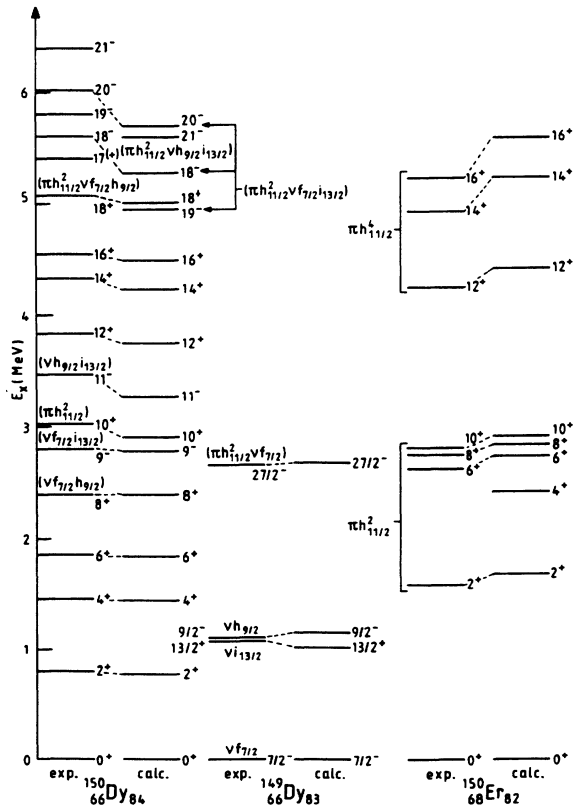

FIG. 12. Comparison between the experimentally observed and calculated excitation energies for the levels in ^{149}Dy, ^{150}Dy, and ^{150}Er. The configurations stated contain the nucleons which are not coupled to $I=0$.

ty of the $\nu(f_{7/2})^2$ and $\pi h_{11/2}\nu f_{7/2}$ residual-interaction and single-particle energies. For the configurations containing an $h_{9/2}$ neutron (8^+, 18^+ in ^{150}Dy and $\frac{9}{2}^-$ in ^{149}Dy), the good agreement merely reflects that the $\pi h_{11/2}\nu h_{9/2}$ interaction has been determined using the excitation energy of these levels. All level energies, which have been calculated using theoretical interaction (Kuo-Herling) energies or the effective $i^*_{13/2}$ interaction energy, show deviations from the experiment. The deviation is largest for the high-spin negative-parity states in ^{150}Dy and is caused by the described Pauli blocking of the particle-hole component in the octupole admixture.

The $\pi(h_{11/2})^4$ residual interaction, calculated from the two-particle residual interaction $\pi(h_{11/2})^2$ determined from the $I=0-10$ levels in ^{148}Dy gives a ground-state mass for ^{150}Er which is about 370 keV too small. Adjusting the calculated value to the 16^+ level energy and not to the ground state, we get good agreement for the 14^+ state and excitation energies which are about 250 keV too small for the lower states. The 0^+ and 2^+ levels in ^{148}Dy, used to determine the $h_{11/2}$-proton interaction, contain admixtures from the neighboring $s_{1/2}$ and $d_{3/2}$ orbitals which could be the reason for the deviations. Therefore, one would expect the best agreement for the $I=14,16$ levels in ^{150}Er, as calculating these levels involves only contributions of the $\pi(h_{11/2})^2$ interaction with a coupling to $I\geq 4$ and $I\geq 6$, respectively, i.e., $([\pi(h_{11/2})^2]_{10^+}\otimes[\pi(h_{11/2})^2]_{4^+,6^+})_{14^+,16^+}$. The calculated levels for nuclei with less valence nucleons than ^{152}Er show the reliability of the single-particle and interaction energies used.

Figure 13 shows the experimental and calculated level energies in ^{152}Er up to spin $I=18$. Due to the $\pi(11/2)^4$ interaction used, the ground-state mass is about 383 eV too low. Adjusting the calculated ground-state mass to the experimental value gives good agreement for the level energies up to the 18^+ level. From the calculations we assign the same configurations to these levels as from the comparison with the neighboring nuclei with fewer valence nucleons. Thus, it is possible to describe the energies of the levels in ^{152}Er up to spin 18 by the shell model with relatively pure configurations.

In Fig. 14 we compare the experimental level energies with the calculated values for still higher states up to the 28^+ isomer. These levels belong to configurations which contain one or two $i_{13/2}$ neutrons. The assignments shown are tentative because of the uncertainties in the single-particle and residual-interaction energies used [due to the octupole admixture $(f_{7/2}\otimes 3^-)_{13/2^+}$ and to the use of mainly theoretical interaction energies]. For the configuration $[\pi(h_{11/2})^4\nu f_{7/2}i_{13/2}]$, i.e., the levels with $I\leq 20$, the calculated energies are too low as in ^{150}Dy. The theoretical values do not consider the mentioned particle-hole component in the octupole admixture and

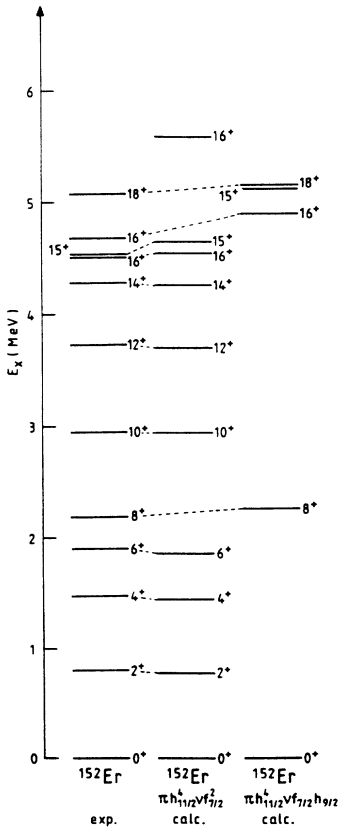

FIG. 13. Comparison between the experimentally observed and calculated excitation energies for the levels up to a spin $I=18$ in ^{152}Er. Stated are the configurations for which the calculations have been done.

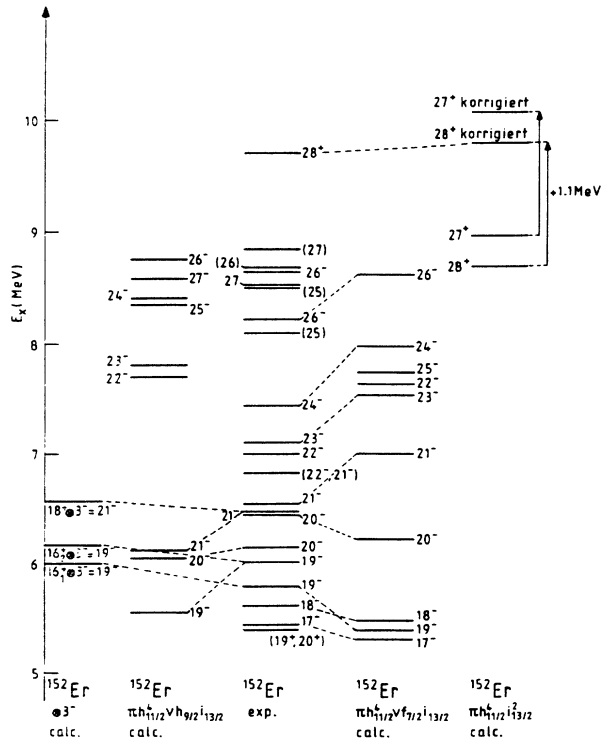

FIG. 14. Comparison between the experimentally observed and calculated excitation energies for the levels above 5 MeV in ^{152}Er. Stated are the configurations for which the calculations have been done.

their interaction with the $h_{11/2}$ protons or the complete blocking of this component for levels with $I \geq 18$. The levels with $I \geq 21$, i.e., where the proton seniority is $v=4$, are calculated at too high an energy. The calculations for the proton levels in ^{150}Er did show that the $\pi h_{(11/2)}^4$ residual interaction overestimates the level energies if one adjusts to the ground state.

In the far left column of Fig. 14 we show the results of a different approach for the calculation of the 19^- and 21^- level energies. Supposing an octupole excitation built on the 16^+ and 18^- levels, respectively, we can determine the expected energy of the 19^- and 21^- levels from the observed excitation energies for the 16^+ and 18^+ levels and the 3^- excitation energy. The latter has been estimated from the systematics of the octupole excitations in the neighboring nuclei, since the 3^- state has not been observed in ^{152}Er. The procedure is comparable with calculating the level energies by using the $i_{13/2}$ single-particle and interaction energies containing the octupole admixture. It is taken into account by using the systematics of the 3^- excitation coupled to the ground state, and the influence of the particle-hole component $[\pi h_{11/2}(d_{5/2})^{-1}]$ is considered assuming a small change for the coupling of the octupole to the 16^+ and 18^+ levels, rather than to the 0^+ ground state.

The 35-ns isomer has a spin $I=28$ and positive parity. This is the maximum possible spin if all six valence nucleons are aligned; therefore, we assume the configuration $[\pi(h_{11/2})^4\nu(i_{13/2})^2]_{28^+}$ for this level. The calculation for this configuration yields too low an excitation energy for the level, as the used $i^*_{13/2}$ single-particle energy, too small by 1.1 MeV, simulates a double octupole admixture for this level while the theoretical $(i_{13/2})^2$ residual interaction used does not contain any portion of a 3^- admixture. In principle, the 28^+ level could be a double octupole excitation built on a $(\pi h^4_{11/2}\nu f^2_{7/2})_{22^+}$ state, similar to the known $\frac{19}{2}^-$ level built on a $\frac{7}{2}^-$ state in ^{147}Gd [26], or the double-octupole excitations known in ^{148}Gd [27] and in ^{150}Gd [28]. For the $I=28$ level in ^{152}Er, the particle-hole component contained in the octupole admixture is blocked for even a single-octupole admixture. In Fig. 14 we show the calculated level at a corrected, 1.1-MeV higher excitation energy, which compensates for one of the $i^*_{13/2}$ single-particle energies used. However, it is an arbitrary correction and does not confirm the stated configuration for the 28^+ level.

The measured half-lives of the two high-spin isomers are not in contradiction with the multipolarities determined for the depopulating transitions and with the proposed configuration for the 28^+ isomer. For the 1265-keV transition, which depopulates the 11-ns isomer at 13.37-MeV excitation energy, the angular correlation result suggests a $\Delta I=3$ transition. The single-particle strength for an $E3$ transition would lead to a half-life of about 165 ns. However, in this mass region, an $E3$ transition can have up to a 50 times larger single-particle strength, as is seen in ^{148}Gd [27].

The 35-ns isomer is depopulated with 50% intensity by the 1051-keV transition, leading to a partial half-life of 70 ns for this transition. According to the angular correlation, it is a mixed $E3/M2$ transition with a mixing parameter of $\delta \approx -1.5$ and thus an $E3/M2$ intensity ratio of $\delta^2=2.25$. Therefore, the partial γ-ray strengths ($T_{sp}=\ln 2/t_{1/2}$) for the components are $T_{sp}(E3)=6.9\times10^6$ s^{-1} and $T_{sp}(M2)=3.1\times10^6$ s^{-1}. The $E3$ component is six times stronger than the $E3$ single-particle strength for this energy while the $M2$ component is strongly hindered. The proposed configurations for the 28^+ and 26^- levels involved are $[\pi(h_{11/2})^4\nu(i_{13/2}2)^2]_{28^+}$ and $[\pi(h_{11/2})^4\nu f_{7/2}i_{13/2}]_{26^-}$, respectively. Hence, this corresponds to a $\nu i_{13/2}\rightarrow\nu f_{7/2}$ transition; an $M2$ transition is not possible, but an admixture of $(\pi h^4_{11/2}\nu h_{9/2}i_{13/2})_{26^-}$ on the order of 4×10^{-3} to the 26^- level could be responsible for the experimentally observed strength for the $M2$ component. The slightly enhanced $E2$ strength is in agreement with the $(f_{7/2}\otimes 3^-)_{13/2^+}$ admixture.

V. CONCLUSIONS

It was possible to extend the ^{152}Er level scheme up to spins of about $I=37$ and to determine the lifetime and depopulation patterns of two high-spin isomers, one of them at an excitation energy of $E_x=13.4$ MeV. The unambiguous determination of the multipolarity was possible for most of the transitions below the 28^+ isomer.

Shell-model calculations show that the yrast structure up to $I=28$ in ^{152}Er can be understood by the coupling of the six valence nucleons outside the ^{146}Gd core. It was possible to calculate the energy for many of the observed levels. This indicates that excitation of the ^{146}Gd core mainly takes place after alignment of the six valence nucleons to a spin of $I=28$. The calculations have been done exclusively for pure spherical configurations built with the six valence nucleons in the $\pi h_{11/2}$, $\nu f_{7/2}$, $\nu h_{9/2}$, and $\nu i_{13/2}$ orbitals. We neglected possible excitations of the core nucleons as well as configuration mixing. For the high-spin levels with negative parity, one could also consider a particle-hole excitation, e.g., $\pi(h_{11/2})^5(d_{5/2})^{-1}\nu(f_{7/2})^2$ or $\pi(h_{11/2})^5(g_{7/2})^{-1}\nu(f_{7/2})^2$. The energy gap above the 24^- and 27^- levels could be an indication for such a core excitation before the maximal possible spin $I=28$ is reached. However, an excitation across the $N=82$ shell closure is energetically unfavored due to the two times larger energy gap compared to the $Z=64$ shell closure.

ACKNOWLEDGMENTS

One of us (A.P.B.) wants to thank the A. v. Humboldt Foundation for financial support. The work was supported by the Bundesminister für Forschung und Technologie BRD.

[1] G. Bastin, A. Pehaire, J. P. Thibaud, S. Andre, D. Barneoud, and C. Foin, Nucl. Phys. **A345**, 302 (1980).
[2] T. Døssing, K. Neergård, Matsuyanagi, and Hsi-Chen Chang, Phys. Rev. Lett. **39**, 1395 (1977); *International Conference on Nuclear Behavior at High Angular Momentum* (Societe francaise de physique, Strasbourg, 1980), Vol. 55.
[3] P. Kleinheinz, R. Broda, P. J. Daly, S. Lunardi, M. Ogawa, and J. Blomqvist, Z. Phys. A **290**, 279 (1979).
[4] J. Pedersen *et al.*, Phys. Rev. Lett. **39**, 990 (1977).
[5] J. Borggreen, S. Bjørnholm, O. Christensen, A. Del Zoppo, B. Herskind, J. Pederson, G. Sletten, F. Folkmann, and R. S. Simon, Z. Phys. A **294**, 113 (1980).
[6] A. Kuhnert, Phys. dissertation, Free University Berlin, Germany, 1988.
[7] M. Guttorsmen, H. Hübel, A. v. Grumbkow, Y. K. Agarwal, J. Recht, M. Menningen, and N. Roy, Nucl. Instrum. Methods **227**, 489 (1984).
[8] H. Backe, L. Richter, R. Willwater, E. Kankeleit, E. Kuphal, Y. Nakagama, and B. Martin, Z. Phys. A **285**, 159 (1978).
[9] C. V. K. Baba, S. Bjørnholm, O. Christensen, B. Herskind, R. M. Lieder, J. Pederson, G. Sletten, F. Folkmann, and R. S. Simon, Phys. Scr. **24**, 290 (1981).
[10] M. H. Rafailovich, O. C. Kittner, A. W. Sunyar, S. Vajda, and G. D. Sprouse, Phys. Rev. C **30**, 169 (1984).
[11] M. Piiparinen, P. Kleinheinz, S. Lunardi, W. Ogawa, G. de Angelis, F. Seramel, W. Meczynski, and J. Blomqvist, Z. Phys. A **337**, 387 (1990); M. Piiparinen *et al.*, Phys. Lett. B **194**, 468 (1987).
[12] P. J. Daly, P. Kleinheinz, R. Broda, S. Lunardi, H. Backe, and J. Blomqvist, Z. Phys. A **298**, 173 (1980).
[13] Y. H. Chung *et al.*, Phys. Rev. C **29**, 2153 (1984).
[14] M. A. Deleplanque, J. C. Bacelar, E. M. Beck, R. M. Diamond, F. S. Stephens, J. E. Draper, Th. Døessing, and K. Keergård, Phys. Lett. B **195**, 17 (1987).
[15] L. G. Mann *et al.*, Lawrence Livermore National Laboratory Report 4-48, 1986.
[16] B. Rubio *et al.*, Z. Phys. A **324**, 27 (1986).
[17] T. T. S. Kuo and G. H. Herling, Naval Research Laboratory Report 2258, 1971.
[18] J. Styczen *et al.*, in *Proceedings of the Fifth International Conference on Nuclei Far from Stability,* Rousseau Lake, Ontario, 1987, edited by Jan S. Towner, AIP Conf. Proc. No. 164 (AIP, New York, 1988), p. 489.
[19] A. Ercan, R. Broda, M. Piiparinen, P. Kleinheinz, and J. Blomqvist, Proceedings of the International Conference on Nuclear Physics, Florence, Italy, 1983 (Tipografia Compositori, Bologna, Italy, 1983), Vol. 1, **B106**, p. 154.
[20] B. Rubio *et al.*, Z. Phys. A **324**, 27 (1986).
[21] A. P. Byrne, G. D. Dracoulis, K. J. Schiffer, P. M. Davidson, T. Kibedi, B. Fabricius, A. M. Baxter, and A. E. Stuchbery, Phys. Rev. C **42**, 6 (1991), and references therein.
[22] H. Kader *et al.*, Phys. Lett. B **227**, 325 (1989).
[23] M. Piiparinen, P. Kleinheinz, S. Lunardi, M. Ogawa, G. de Angelis, F. Soramel, W. Meczynski, and J. Blomqvist, Z. Phys. A **337**, 387 (1990).
[24] M. Lach, P. Kleinheinz, M. Piiparinen, M. Ogawa, S. Lunardi, M. C. Bosca, J. Styczen, and J. Blomqvist, Z. Phys. A **341**, 25 (1991).
[25] R. Broda, M. Behar, P. Kleinheinz, P. J. Daly, and J. Blomqvist, Z. Phys. A **293**, 135 (1979).
[26] P. Kleinheinz, J. Styczen, M. Piiparinen, J. Blomqvist, and M. Kortelahti, Phys. Rev. Lett. **48**, 1457 (1982).
[27] S. Lunardi, P. Kleinheinz, M. Piiparinen, M. Ogawa, M. Lach, and J. Blomqvist, Phys. Rev. Lett. **53**, 1531 (1984).
[28] D. R. Haenni and T. T. Sugihara, Phys. Rev. C **16**, 120 (1977).